

On the checkerboard pattern and the autocorrelation of photoemission data in high temperature superconductors

E. Bascones and B. Valenzuela

*Instituto de Ciencia de Materiales de Madrid, CSIC. Cantoblanco. E-28049 Madrid, Spain**

(Dated: February 8, 2020)

The joint density of states of $\text{Bi}_2\text{Sr}_2\text{CaCu}_2\text{O}_{8+\delta}$, obtained from the autocorrelation of angle resolved photoemission data, presents^{1,2}, respectively in the superconducting and pseudogap states, dispersive and non-dispersive peaks in momentum space, which compare well with those reported from STM experiments. The non-dispersive features, presumably responsible for the checkerboard pattern found in STM, arise from the tips of the Fermi arcs. Here we show that these photoemission experiments can be understood within a model for the pseudogap with no charge-ordering or symmetry breaking. We assume that superconductivity and pseudogap coexist in the superconducting state and predict the presence of both kind of peaks in the superconducting state of underdoped cuprates. We propose that the checkerboard substructure can be explained within the same picture and argue that the cuprates with low critical temperatures are good candidates for experiments.

In the pseudogap (PG) state of underdoped cuprates instead of a complete Fermi surface³, just a Fermi arc around the nodal (diagonal) direction is seen, while the antinodal region close to $(\pi, 0)$ is gapped. Raman⁴ and photoemission^{5,6,7} experiments have shown that the nodal-antinodal dichotomy persists in the superconducting (SC) state, what can be explained in terms of the coexistence of superconductivity and PG correlations below the critical temperature (T_c) and their competition for phase space⁸. Interesting behavior has been also uncovered by Fourier transform scanning tunneling spectroscopy (FT-STS)^{9,10,11,12,13,14,15,16,17,18}. FT-STS gives information on the momentum \mathbf{q} and energy ω dependent density of states $n(\mathbf{q}, \omega)$. Peaks in $n(\mathbf{q}, \omega)$ in momentum space, both dispersive^{10,11,14} and non-dispersive^{9,12,13,14,15,16,17,18} with binding energy, have been detected. The dispersive features appear in the SC state and are believed to be consequence of quantum interference of quasiparticles by elastic scattering^{19,20,21}. In this picture, maxima in $n(\mathbf{q}, \omega)$ are expected at those momenta which connect states with the largest joint density of states (JDOS). In the so-called octet model¹⁹, in the SC state the largest density of states at a given ω is found at the tips of the banana-shaped constant energy contours around the nodes (see Fig. 1b) and $n(\mathbf{q}, \omega)$ peaks at the wavevectors $\mathbf{q}_1, \dots, \mathbf{q}_7$ (and the eightfold symmetric ones) which connect such tips.

More controversial is the origin of the non-dispersive features, also referred as checkerboard pattern. The checkerboard pattern has been observed in the SC state at the vortex core⁹ and at zero field^{13,14} and in the PG state^{12,13}. Peaks in $n(\mathbf{q}, \omega)$ appear at $\mathbf{q} \sim (\pm 2\pi/\lambda, 0)$ and $(0, \pm 2\pi/\lambda)$ in units of the lattice spacing, with $\lambda \sim 4-5$, and no measurable change of the characteristic momentum with energy. Together with this modulation, weaker substructure at $\mathbf{q} \sim (\pm 3(2\pi)/4, 0)$ and $(0, \pm 3(2\pi)/4)$ has been detected^{13,14,15,16,17}. Theoretical efforts have been concentrated on the $\lambda \sim 4-5$ pattern with little attention to the substructure. Due to its non-dispersive nature²², most of the models are based on inhomogeneous states involving charge ordering, static^{13,23,24,25,26,27,28,29,30,31} or

incipient³². Proposals based on the JDOS picture have been also discussed^{22,33}. At the heart of this debate underlies the key for PG.

The interpretation of FT-STS experiments is complicated by the influence of the disorder model, the approximation used or unknown matrix elements effects. On the other hand, the JDOS picture can be checked³⁴ autocorrelating angle-resolved photoemission (ARPES) data. Neglecting the matrix element, ARPES measures the spectral function $A(\mathbf{k}, \omega)$. The JDOS is obtained from the convolution $JDOS(\mathbf{q}, \omega) = \sum_k A(\mathbf{k}, \omega)A(\mathbf{k} + \mathbf{q}, \omega)$. The \mathbf{q} -space pattern measured from the autocorrelation of ARPES (AC-ARPES) data can be directly interpreted, as it does not require any theoretical modelling. Dispersive and non-dispersive peaks in AC-ARPES in the SC and PG states respectively, which compare well with those measured by FT-STS, have been recently detected^{1,2} in $\text{Bi}_2\text{Sr}_2\text{CaCu}_2\text{O}_{8+\delta}$ (Bi2212). In the PG state above T_c AC-ARPES data presents² peaks near $(0.4\pi, 0)$ with very little dispersion, in contrast to the ones in the SC state. They are associated to vectors of the \mathbf{q}_1^* type in Fig. 1a), connecting the tips of the Fermi arcs. Peaks corresponding to \mathbf{q}_5^* in Fig. 1a) and structure along the diagonal are also observed. These results point to a JDOS explanation of the checkerboard pattern and cast doubt on those models involving charge ordering. At least in the SC state¹, AC-ARPES data along the diagonal peaks also at the internodal vector \mathbf{P}_N .

In this letter we analyze the AC-ARPES spectra of the model recently proposed by Yang, Rice and Zhang (YRZ) for the pseudogap³⁵. It is assumed that PG and superconductivity coexist below T_c and a critical doping x_c . In agreement with experiments we find clearly dispersive peaks in the SC state while peaks with very little dispersion (referred as non-dispersive in the following) appear in the PG. Both kind of peaks are present at low doping x in the SC state. The dispersive ones are restricted to low energies, lower with underdoping. The non-dispersive features in the SC state dominate the spectrum at small doping and are a consequence of the persistence of PG correlations below T_c and its imprint

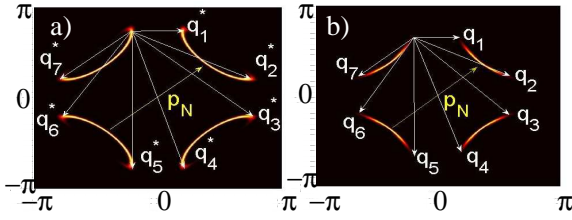


FIG. 1: (color online) (a) ARPES intensity around the nodes in the pseudogap state for $\omega = -0.04$, in units of the bare nearest neighbor hopping, and $x = 0.16$ according to the model discussed. (b) Same as in (a) in the superconducting state for $x = 0.20$. The wavevectors \mathbf{q}_i (\mathbf{q}_i^*) of quasiparticle interference patterns in the octet model, as well as the intranodal momenta along the diagonal \mathbf{P}_N .

on the spectral function and energy dispersion. Along the diagonal, both the peaks corresponding to \mathbf{q}_7 and \mathbf{q}_3 (\mathbf{q}_7^* and \mathbf{q}_3^*), included in the octet model, in Fig. 1, and strong intensity at \mathbf{P}_N due to nesting, appear.

In the YRZ model PG correlations are given³⁵ by Δ_R . Δ_R decreases with doping x and vanishes at a topological quantum critical point x_c . Instead of a large Fermi surface, hole pockets appear close to $(\pm\pi/2, \pm\pi/2)$. Their size increases with larger x . Due to reduced spectral weight on the outer edge of the pocket, a gapless Fermi arc appears in ARPES at zero energy^{8,35}. At finite energy the arc structure, shown in Fig. 1b, remains. The pocket formation at finite Δ_R happens without breaking the symmetry. The SC order parameter Δ_S is related to T_c . The model has been only developed for zero temperature. The PG state is characterized by zero Δ_S and finite Δ_R . In the SC state, the arc is gapped. Both Δ_R and Δ_S have d-symmetry $\Delta_\alpha(\mathbf{k}) = \Delta_\alpha(x)(\cos k_x - \cos k_y)$ with $\alpha = R, S$, but they gap the Fermi surface in a different way³⁵. Beyond x_c a complete Fermi surface and BCS behavior is recovered.

Our aim is not to fit the experiments but to discuss the main features in the AC-ARPES spectra and why do they appear. Thus, we take exactly the same parameters for Δ_S , Δ_R and the band dispersion proposed in the original paper³⁵ and used afterwards⁸. In particular, we use the following doping dependences: $\Delta_R(x)/2 = 0.3(1 - x/0.2)$ and $\Delta_S(x)/2 = 0.07(1 - 82.6(x - 0.2)^2)$. Energies are measured in units of the bare nearest neighbor hopping $t_0 \sim 300 - 400$ meV. With these dependences on doping, $x_c = 0.2$, the doping at which Δ_R vanishes, coincides with the doping with largest Δ_S but this may not be the case experimentally. The anomalous behavior, i.e. the emergence of non-dispersive features, is expected below x_c . The exact expressions for the spectral function and energies of the YRZ model have been given elsewhere^{8,35} and we do not repeat them here. In order to compare with experiments we autocorrelate the computed spectral function following the same procedure as in refs^{1,2}. Only those momenta \mathbf{k} which satisfy that both \mathbf{k} and $\mathbf{k} + \mathbf{q}$ belong to the first Brillouin zone are included in the sum. Umklapp terms do not enter and the autocor-

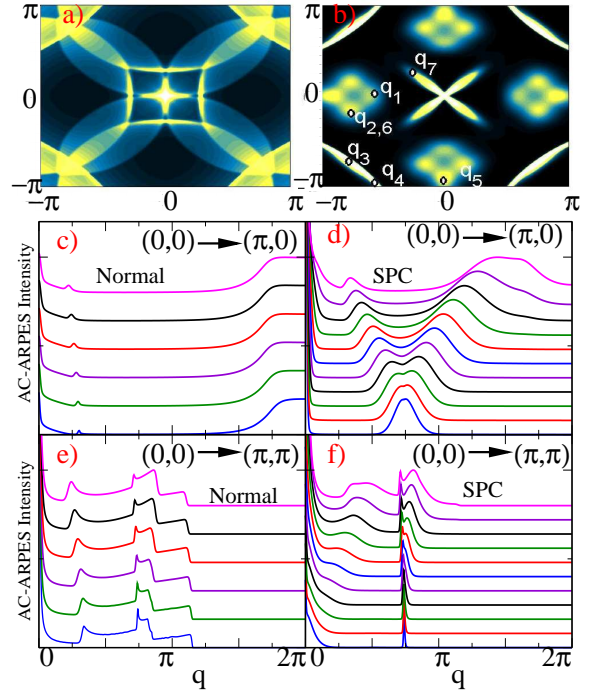


FIG. 2: (color online) AC-ARPES spectra for $x_c = 0.20$ ($\Delta_R = 0$). a) and b) respectively show, in arbitrary units, the maps at $\omega = -0.04$ in the normal ($\Delta_S = 0$) and superconducting ($\Delta_S = 0.14$) state. c) and e) Intensity of the autocorrelated spectral function along the $(0, 0) - (\pi, 0)$ and $(0, 0) - (\pi, \pi)$ directions respectively in the normal state at several energies. From bottom to top $\omega = -0.10$ in 0.02 intervals and in units of the bare nearest neighbor hopping. d) and f) respectively the same as c) and e) but in the superconducting state at energies, from bottom to top $\omega = -0.10$ at 0.01 intervals. Each curve in c) to f) is normalized to the value at its largest feature other than the one at $(0, 0)$ and displaced, to better show the dispersion of the peaks.

related spectra does not have the lattice symmetry. To mimic finite energy-resolution in ARPES, the spectral function is convoluted with a gaussian of width $0.02t_0$.

We start discussing the AC-ARPES spectra for $x_c = 0.20$, doping at which PG correlations vanish and standard Fermi liquid and BCS behaviors are expected. AC-ARPES maps in the normal and SC states are shown in Fig. 2a and 2b for $\omega = -0.04$. Fig. 2b closely resemble the ones obtained from experimental data^{1,2} in the SC state. It also remember those arising from the convolution of the Green function with itself discussed in the context of STM experiments^{19,20} but it lacks the kaleidoscopic patterns due to umklapp²⁰ present in the latest. In the SC state the spectra peaks at $\mathbf{q} = (0, 0)$ and disperses towards the diagonal due to *intranodal* \mathbf{q}_7 -type terms in Fig. 1b. Features related to *internodal* $\mathbf{q}_{1,5}$, and $\mathbf{q}_{2,6}$ autocorrelations are found at and close to the $(0, 0) - (\pm\pi, 0)$ and $(0, 0) - (0, \pm\pi)$ directions and others of the $\mathbf{q}_{3,4}$ kind appear close to $(\pm\pi, \pm\pi)$. Further insight is obtained from Figs. 2d and 2f, which respectively show the intensity along $(0, 0) - (\pi, 0)$ and $(0, 0) - (\pi, \pi)$

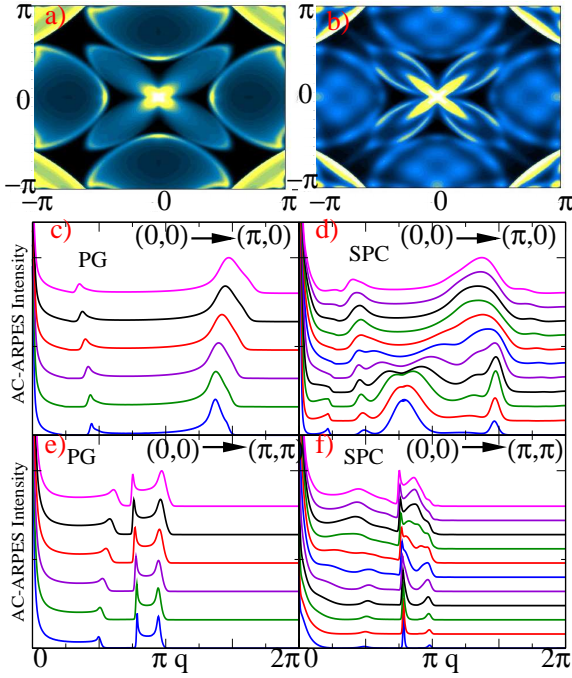


FIG. 3: (color online) Same as in Fig. 2 but for $x = 0.16$ in the pseudogap (left) and superconducting state (right). $\Delta_R = 0.12$ in both cases and $\Delta_S = 0.12$ in the latest one.

for several energies in the SC state. In Fig. 2d the peak at $\mathbf{q} \sim (0.75\pi, 0)$ at zero energy splits at finite energy into two peaks with a clear dispersion. The feature at smaller (larger) momentum comes from \mathbf{q}_1 (\mathbf{q}_5) autocorrelation contributions. In the $(0, 0) - (\pi, \pi)$ direction at zero energy there is a sharp peak at $\mathbf{q} \sim (0.75\pi, 0.75\pi)$. Instead of just dispersing with increasing momenta, as \mathbf{q}_3 does, it splits. The extra and almost dispersionless peak is due to nesting²⁰ and corresponds to \mathbf{P}_N -like internodal contributions, as also seen by McElroy *et al*¹. It is also present in Fig. 2e in the normal state. The broad dispersive feature in Fig. 2f close to $(0, 0)$ can be associated to \mathbf{q}_7 momenta. The onset of \mathbf{q}_3 and \mathbf{q}_7 contributions at the edges of the Brillouin zone results in the step like features in Fig. 2e at momenta respectively slightly larger and smaller than (π, π) . Good nesting at the antinodal region favors peaks at small momenta both at the diagonal and along the $(0, 0) - (\pi, 0)$ direction and is responsible for the flat maxima at $(2\pi, 0)$ in Fig. 2c.

We turn now to the more interesting case with finite Δ_R , plotted in Fig. 3. At first sight the ARPES intensities in the the BCS superconducting and the PG states in Fig. 1 look similar. But their AC-ARPES spectra and energy-dependence show important differences. At zero energy the Fermi arc length is finite and contrary to what happens in the SC case the \mathbf{q}_1^* and \mathbf{q}_5^* features in the ARPES spectrum are split in Fig. 3c, even at zero energy. Their momenta and energy dependence resemble that found in the PG state by Chatterjee *et al*². Their positions change very little with energy in strong contrast

to the dispersive behavior in Fig. 2d). This weak dispersion could be reduced by finite lifetimes, weaker spectral weight at the antinode or a worse experimental resolution than included here. Similar zero-energy splitting and non-dispersing behavior appears along the diagonal in Fig. 3d. The stronger peaks come from \mathbf{P}_N and \mathbf{q}_3^* terms and the weaker one at smaller momenta from \mathbf{q}_7^* .

Dispersive behavior at low energies appears in the SC state even for finite Δ_R . Interestingly, both dispersive and non-dispersive features can be distinguished in Fig. 3d. The opening of the gap in the arcs suppresses the non-dispersive peaks arising from the tips of the arcs but remanent structure is visible at the corresponding momenta. Dispersive peaks, of the type observed in Fig. 2, dominate at low energy but there is a clear kink in the dispersion and the peaks converge to those observed in the PG state. This is better seen in Fig. 4a, where the position of the maxima is plotted. We note that dispersive peaks at low energies and non dispersive ones at higher energies have been observed in FT-STS experiments in underdoped Bi2212¹⁴.

The energy at which the change from dispersive to non-dispersive behavior happens is mainly given by $\Delta_S(\mathbf{k})$ at the arc tip, which is controlled by Δ_R . Overlap of dispersive and non-dispersive peaks does not always allow to distinguish between them or to associate the position of the maximum in intensity to specifically one of these features. The AC-ARPES spectra, corresponding to $x = 0.12$ and $x = 0.18$ in the SC state along the $(0, 0) - (\pi, 0)$ direction are shown in Figs. 4b and 4c. Δ_S and Δ_R are finite in both cases. However, dispersive and non-dispersive peaks are not as clearly identified here as they were in Fig. 3d. For $x = 0.12$ the dispersive peaks cannot be distinguished above $|\omega| = 0.01$ and the spectra looks like the one in the PG (not shown). On the contrary, for $x = 0.18$ Δ_R is small and the dispersion resembles the one found in the SC beyond x_c . The presence of only dispersive (non-dispersive) peaks does not ensure that Δ_R (Δ_S) is zero.

On the other hand, for smaller $\frac{\Delta_S}{\Delta_R}$ the non-dispersive structure is more pronounced and for a given doping, the range of energies at which dispersive features appear is reduced with decreasing Δ_S . In agreement with recent ARPES measurements⁷, we expect Δ_S to be to some extent related to T_c . Based on this argument, we predict that the peaks in the AC-ARPES spectra of superconducting $\text{Ca}_{2-x}\text{Na}_x\text{CuO}_2\text{Cl}_2$ (Na-CCOC) or $\text{Bi}_2\text{Sr}_2\text{CuO}_{6+\delta}$ (Bi2201) will be mostly non-dispersive, similar to the ones found in the PG state in Bi2212². We note that in FT-STS experiments in the SC state, the checkerboard pattern is better seen in cuprates with low T_c and when the integrated density of states lacks the coherence peaks, when it is more PG like^{13,14,16,17}. In fact, to the best of our knowledge dispersive features have been seen so far only in Bi2212^{10,11,14}, and not in low- T_c cuprates as Na-CCOC¹³ or $\text{Bi}_2\text{Sr}_{1.6}\text{La}_{0.4}\text{CuO}_{6+\delta}$ (Bi2201-La)¹⁷. In our view, the checkerboard structure found by FT-STS in Na-CCOC and in Bi2212 have a

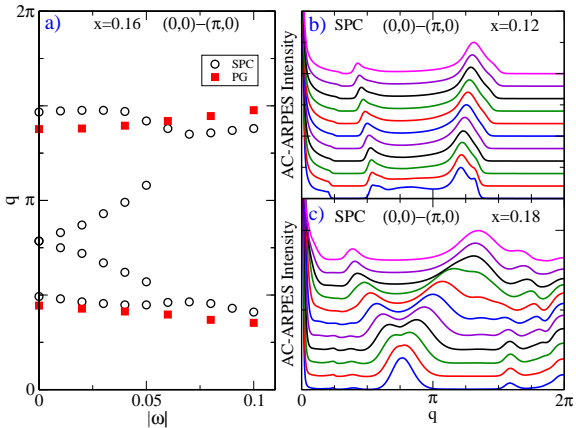


FIG. 4: (color online) a) Position of the dispersing and non-dispersing peaks found in the $(0,0) - (\pi,0)$ direction in the superconducting and pseudogap state at $x = 0.16$. b) and c) Same as in Fig. 3d) but for $x = 0.12$ ($\Delta_R = 0.24$, $\Delta_S = 0.07$) and $x = 0.18$ ($\Delta_R = 0.06$, $\Delta_S = 0.13$) respectively.

common origin, given by the JDOS discussed above. We also note that the momenta at which the weaker substructure has been observed¹³ is very close to the one at which the \mathbf{q}_5^* peak is found, and we postulate that both features are related. In our model, as well as in AC-ARPES experiments², but so far not in FT-STS, non-dispersive peaks are present not only along the $(0,0) - (\pi,0)$, but also along the diagonal. It has been speculated^{1,36} that matrix element effects could suppress tunneling into states near the zone diagonal and prevent^{1,2} the appearance of these peaks in FT-STS experiments. While this issue requires further study, we note that on spite of the consensus on the origin of the FT-STS dispersive peaks and the complicated disorder models considered²¹, discrepancies between theory and experiment persist. It seems specially difficult to explain the predominance of the \mathbf{q}_1 peak along the Cu-O bond

with respect to the \mathbf{q}_7 one along the diagonal direction.

We caution that while we believe that the FT-STS features have a JDOS origin, the autocorrelation of the spectral function is not expected to reproduce $n(\mathbf{q}, \omega)$. As extensively discussed^{19,20,21,33}, the modulations of the density of states induced by quasiparticle interference depend on the coherence factors, the magnetic character of the impurities and the type of disorder. Experimental AC-ARPES spectra is also influenced by the anisotropic and energy dependent lifetime not included here.

Recent ARPES experiments³⁷ have suggested that in the PG state the Fermi length is temperature dependent and vanishes at low temperatures, while the antinodal region remains gapped up to the PG temperature. The observation by Chatterjee *et al*² that the nondispersive peaks found in the AC-ARPES in the PG state arise from the tips of the Fermi arcs and that a SC-type gap in the arcs results in dispersive features, opens a new way to get complementary information on the length and change of the Fermi arcs at both zero and finite energies as the temperature or other parameters like doping change. We believe that low T_c cuprates are the most suitable for this experiment as the two scales will differ more and even underdoped non-SC samples, showing the checkerboard pattern, are available¹³.

In conclusion, we have shown that the non-dispersive structure found in the autocorrelation of photoemission data in Bi2212 in the pseudogap state can be explained without involving charge ordering or symmetry breaking. We predict that depending on doping and T_c both dispersing and non-dispersing peaks can be found in the AC-ARPES spectra in the superconducting state of underdoped cuprates. New experiments are proposed.

We acknowledge funding from MEC through FIS2005-05478-C02-01 and Ramon y Cajal and from Consejería de Educación de la Comunidad de Madrid and CSIC through 200550M136 and I3P.

- * Electronic address: leni@icmm.csic.es, belenv@icmm.csic.es
- ¹ K. McElroy *et al.*, Phys. Rev. Lett. **96**, 067005 (2006).
- ² U. Chatterjee *et al.*, Phys. Rev. Lett. **96**, 107006 (2006).
- ³ M.R. Norman *et al.*, Nature **392**, 157 (1998).
- ⁴ M. Le Tacon *et al.*, Nature Physics **2**, 138 (2006).
- ⁵ K. Tanaka *et al.*, Science **314**, 1910 (2006).
- ⁶ M. Hashimoto *et al.*, cond-mat/0610758.
- ⁷ T. Kondo *et al.*, cond-mat/0611517.
- ⁸ B. Valenzuela and E. Bascones, cond-mat/0611154.
- ⁹ J.E. Hoffman *et al.*, Science **295**, 466 (2002).
- ¹⁰ J.E. Hoffman *et al.*, Science **297**, 1148 (2002).
- ¹¹ K. McElroy *et al.*, Nature (London) **422**, 592 (2003).
- ¹² M. Vershinin *et al.*, Science **303**, 1995 (2004).
- ¹³ T. Hanaguri *et al.*, Nature (London) **430**, 1001 (2004).
- ¹⁴ K. McElroy *et al.*, Phys. Rev. Lett. **94**, 197005 (2005).
- ¹⁵ G. Levy *et al.*, Phys. Rev. Lett. **95**, 257005 (2005).
- ¹⁶ A. Hashimoto *et al.*, Phys. Rev. B **74**, 064508 (2006).

- ¹⁷ T. Machida *et al.*, J. Phys. Soc. Japan **75**, 083708 (2006).
- ¹⁸ C. Howald *et al.*, Phys. Rev. B **67**, 014533 (2003).
- ¹⁹ Q.-H. Wang and D.-H Lee, Phys. Rev. B **67**, 020511 (2003).
- ²⁰ L. Capriotti, D.J. Scalapino and R.D. Sedgewick, Phys. Rev. B **68**, 014508 (2003). T. Pereg-Barnea and M. Franz, Phys. Rev. B **68**, 180506 (2003).
- ²¹ L. Zhu, W.A. Atkinson and P.J. Hirschfeld **69**, 060503 (2004). T. Nunner *et al.*, Phys. Rev. B **73**, 104511 (2006).
- ²² Misra *et al.*, Phys. Rev. B, **70**, 220503 (2004).
- ²³ H.-D. Chen *et al.*, Phys. Rev. Lett. **89**, 137004 (2002).
- ²⁴ Z. Tesanovic, Phys. Rev. Lett. **93**, 217004 (2004).
- ²⁵ A. Polkovnikov, M. Vojta and S. Sachdev, Phys. Rev. B **65**, 220509 (2002).
- ²⁶ D. Podolsky *et al.*, Phys. Rev. B **67**, 094514 (2003).
- ²⁷ M. Vojta, Phys. Rev. B **66**, 104505 (2002).
- ²⁸ P.W. Anderson, cond-mat/0406038.
- ²⁹ F.J. Ohkawa, Phys. Rev. B **73**, 092506 (2006).

³⁰ C. Li, S. Zhou and Z. Wang **73**, 060501 (2006).

³¹ J.X Li, C.Q Wu, D.H. Lee, Phys. Rev. B **74**, 184429 (2006).

³² L. Dell'Anna *et al*, Phys. Rev. B **71**, 064518 (2005).

³³ C. Bena *et al*, Phys. Rev. B **69**, 134517 (2004). A. Ghosal, A. Kopp, S. Chakravarty, Phys. Rev. B **72**, 220502 (2005).

³⁴ R.S. Markiewicz Phys. Rev. B **69**, 214517 (2004).

³⁵ K-Y Yang, T.M. Rice and F-C Zhang, Phys. Rev. B **73**, 174501 (2006).

³⁶ C. Wu, T. Xiang, Z-B. Su, Phys. Rev. B **62**, 14427 (2000).

³⁷ A. Kanigel *et al*, Nature Phys. **2**, 447 (2006)